Chapter 3

Low-Noise Operation of Mid-Infrared Quantum Cascade Lasers Using Injection Locking

Hercules Simos, Adonis Bogris and Dimitris Syvridis

Additional information is available at the end of the chapter

http://dx.doi.org/10.5772/66941

Abstract

Quantum cascade lasers are the most promising optical source for emission in the mid-infrared and THz region, and they are already used in a large number of applications such as free-space communications, absorption spectroscopy, sensing and so on. In all these applications, the noise properties of the optical sources are critical for the system performance. In this work, the authors present a theoretical study on the intensity noise characteristics of quantum cascade lasers (QCLs) under external non-coherent optical injection. The injection locking has been proven in the past beneficial for noise properties of bipolar lasers, and thus this technique is utilized here in quantum cascade lasers. With the help of various analytical and numerical models, it is shown that intensity noise reduction can be achieved in the operation of the so-called locked slave laser compared to its free-running values. The detailed analysis reveals the contribution of the various noise sources to the intensity noise of the laser and how they affect the injection locking process. Using different numerical models, two distinct schemes are investigated, analysed and discussed, injection on the lasing mode or on non-lasing residual modes of the slave laser cavity.

Keywords: quantum cascade laser, optical injection locking, noise

1. Introduction

Quantum cascade lasers (QCLs) are a relatively new class of optical sources exploiting radiative intersubband transitions in semiconductor heterostructures, giving operation in a wide range of wavelengths, from 3.5 to 150 μm [1]. After the demonstration of the first QCL in

1994 [2], there has been huge effort for the implementation of sources similar to the ones commonly used in the infrared regime, like single-mode or powerful tunable lasers for either continuous wave or pulsed operation at room temperature (RT). Today, QCL technology is the dominant source for emission in the mid-infrared and THz region. The mid-infrared spectral region hosts a large number of applications including free-space communications, absorption spectroscopy, chemical and biological sensing, and LIDAR (LIght Detection and Ranging) applications. Although QCL technology has reached a certain degree of maturity, many of their physical properties such as the modulation, noise and nonlinear properties are still under investigation and progress, leading to many important contributions in the field. Especially, the noise properties of QCLs are extremely important for spectroscopy and sensing applications as they define the system sensitivity.

Strong effort has been put to identify the specific properties that differentiate these devices from their interband counterparts, the diode lasers, which emit in the near infrared regime [3–7]. In this context, mature techniques from the near infrared wavelength region have been adopted in the mid infrared region to provide insight in the operation and optimize the emission characteristics of QCLs and related systems. One of these techniques, the optical injection locking (OIL) has been investigated extensively for classic (interband) diode lasers in order to exploit its fundamental property of phase synchronization between two independent laser sources [8]. In OIL, a laser source which is considered as "slave" is optically injected by a second "master" laser, and as a result of the locking procedure, the slave laser emits at the wavelength of the master laser and follows its phase fluctuations. Apart from this fundamental property, OIL has been also proposed and utilized in order to demonstrate amplitude noise and phase noise squeezing [9]. In the mid infrared region, the intensity noise of injection-locked QCLs was recently investigated theoretically and experimentally [10, 11], and the obtained results revealed the potential of the locked (slave) laser to operate under reduced intensity noise levels compared to the free-running operation. From the application point of view, absorption spectroscopy would substantially benefit from this reduction of the laser intensity noise, which leads to higher signal-to-noise ratios and thereby enables lower detectable concentrations in corresponding absorption experiments.

In this chapter, the authors analyse the emission characteristics of mid infrared injection-locked QCLs in terms of the intensity noise using theoretical numerical models. The analysis has the following stages. First, a review of the developed computational tools for the proper description of the operation and various aspects of QCLs, such as the noise characteristics and the modulation properties, is carried out. Second, the investigation of the intensity noise characteristics of free-running QCLs, which serves as a calibration/optimization tool for the various numerical models. The third part focuses on the noise performance of injection-locked QCLs and how it is affected by the system parameters. For the injection-locked QCLs, two separate cases are considered, the single-mode scheme (injection in a single-mode slave laser) and the multimode scheme (injection on the main or side modes of a multimode slave laser). Furthermore, special cases for optimized low-noise operation are identified and discussed.

http://dx.doi.org/10.5772/66941

2. Numerical tools

2.1. Rate equation models

The numerical rate equation (RE) models are based on the assumption of the laser homogeneity in the spatial coordinate (direction of propagation) and thus provide a very efficient calculation tool for the dynamics of interband single-mode semiconductor lasers [like Distributed Feedback Lasers (DFB), external cavity lasers, etc]. Lately, RE models have been modified and used to study the emission characteristics of intersubband QCLs. Such a RE model is utilized for the investigation of the intensity noise of single-mode QCLs [12] and presented below.

For the purposes of the noise investigation, the band structure of a QCL is described with a three-level approximation, and it is shown in **Figure 1**. As usually, several assumptions have been made in order to simplify the sophisticated energy structure of the quantum well of each stage. Photons are emitted during a carrier transition from level 3 to level 2, whereas optical phonon emission occurs at the transition from level 2 to level 1. It is assumed that the electrons from the injector of the previous stage are received by energy

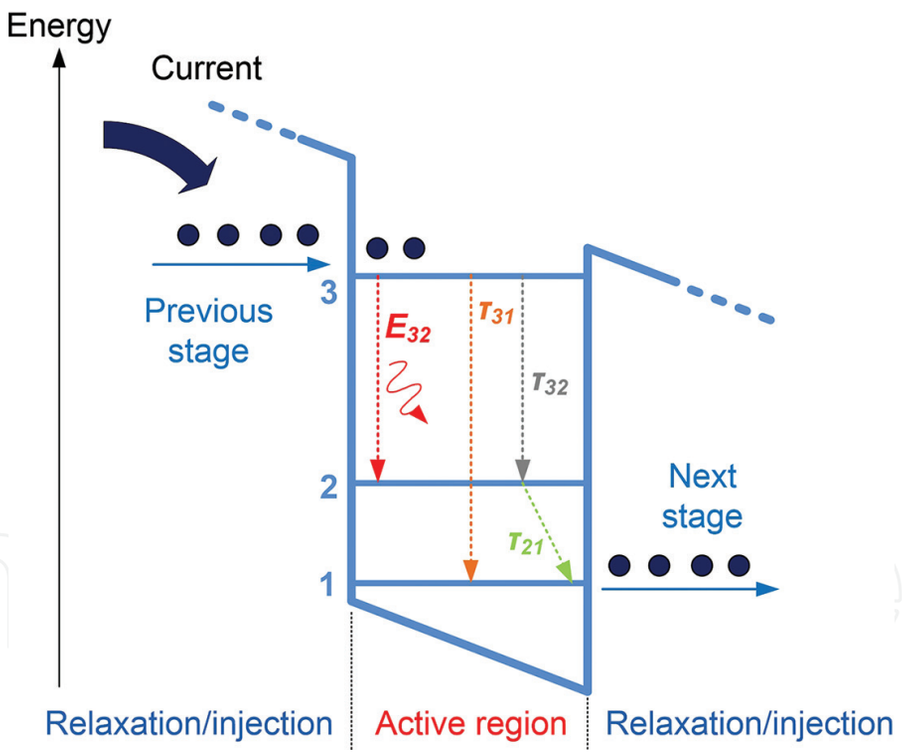

Figure 1. Schematic of the three-level energy band structure of the mid-infrared quantum cascade laser (QCL) considered for the noise investigation.

level 3, and the electrons from level 1 relax to the miniband and injector of the next stage. The radiative and non-radiative transitions from level 3 to levels 2 and 1 are also taken into account. The carrier and photon dynamics are described by rate equations for the carrier

number population for each level and the photon number. The RE system assuming single-mode operation reads [12, 13]:

$$\frac{dN_3}{dt} = \frac{\eta I}{q} - \frac{N_3}{\tau_{32}} - \frac{N_3}{\tau_{31}} - g(N_3 - N_2)S + F_3 \tag{1}$$

$$\frac{dN_2}{dt} = \frac{N_3}{\tau_{32}} - \frac{N_2}{\tau_{21}} + g(N_3 - N_2)S + F_2 \tag{2}$$

$$\frac{dN_1}{dt} = \frac{N_3}{\tau_{31}} + \frac{N_2}{\tau_{21}} - \frac{N_1}{\tau_{\text{out}}} + F_1 \tag{3}$$

$$\frac{dS}{dt} = Zg(N_3 - N_2)S + Z\beta\frac{N_3}{\tau_e} - \frac{S}{\tau_{\text{ph}}} + F_S \tag{4}$$

In Eqs. (1)–(4), $N_i = N_i(t)$ is the carrier number at the energy level i (i = 1, 2, 3), $S = S(t)$ is the photon number, g the gain coefficient, β is the coupling of the spontaneous emission to the optical mode and Z is the number of cascaded stages. The time constants: τ_{ph} is the photon lifetime; τ_e is the carrier recombination time and τ_{ij} the energy-level transition characteristic times. Finally, I is the injection current and η is the current injection efficiency. Also, it is assumed that all electrons which move from the stage to the injector escape to the next stage. The terms $F_i = F_i(t)$ (i = 1, 2, 3, S) represent the noise contribution based on the Langevin force formulation including the various noise correlations; appropriate expressions can be found in Ref. [12]. Taking into account all the non-zero correlations properly, results in a complicated nonlinear system which is difficult to treat numerically. However, analytical calculations of the relative intensity noise (RIN) spectrum based on the RE system (1)–(4) and presented in Ref. [12] identified the separate contribution of each noise term. The results revealed that the dominant contributions to the total RIN come from the carriers in level 3 and the photons, as also confirmed by the experimental results in Ref. [14]. Thus for the usual operating conditions, the cross-correlation terms can be neglected, and the numerical solution of the RE system is simplified. Based on the above assumption, throughout this study, the noise terms F_3, F_2 and F_S have been taken into account assuming the correlations of [12]:

$$\langle F_3 F_3 \rangle = 2\left(g N_3 S + \frac{N_3}{\tau_e}\right) = 2D_{33} \tag{5}$$

$$\langle F_2 F_2 \rangle = 2\left(g N_3 S + \frac{N_3}{\tau_{32}}\right) = 2D_{22} \tag{6}$$

$$\langle F_S F_S \rangle = 2Z\left(g N_3 S + \beta\frac{N_3}{\tau_e}\right) = 2D_{SS} \tag{7}$$

The coefficients D_{ij} represent the correlation strength between the various noise terms. The noise sources F_3, F_2 and F_S in Eqs. (1)–(4) are calculated by

$$F_i = F_i(t) = \sqrt{\frac{2D_{ii}}{dt}}\, x_i \tag{8}$$

http://dx.doi.org/10.5772/66941

In Eq. (8), dt is the integration time step used here to determine the noise bandwidth, and x_i (i = 3, 2, S) are independent random Gaussian variables with zero mean value and unit standard deviation.

In order to account for the phase information of the fields which is critical in the injection locking process, the model has been modified: the photon number and the phase have been replaced by the complex field. The time evolution of the field [Eq. (9)] arises from the transformation of Eq. (4) as in Ref. [15]:

$$\frac{dE}{dt} = \frac{1}{2}\left[Zg(N_3 - N_2) - \frac{1}{\tau_{\text{ph}}}\right](1 + i\,\alpha_{LEF})E + E_{sp} + \frac{\sqrt{\kappa_{inj}}}{\tau_r}E_{inj} - \text{i}\delta\omega\text{E} \tag{9}$$

Here $E = E(t)$ is the complex field normalized in terms of photon number ($|E|^2 = S$). The phase change is introduced through the linewidth enhancement factor (α_{LEF}). The spontaneous emission E_{sp} is a complex number and it is given by

$$E_{sp} = \sqrt{\frac{1}{2dt}Z\left(g\,N_3 + \beta\frac{N_3}{\tau_e S}\right)}(x + iy) \tag{10}$$

where x and y are random Gaussian variables with zero mean value and unit standard deviation. Equation (10) has been derived following the procedure in Ref. [15].

The two last terms on the r.h.s. of Eq. (9) represent the injection locking process in which a "master" laser is injected into the "slave" laser [16]. E and E_{inj} are the fields of the slave and the master laser, respectively, and their frequency difference is $\delta\omega = 2\pi \cdot df$. The power injection ratio κ_{inj} is defined as the optical power ratio of the master to free-running slave laser (P_{inj}/P). τ_r is the round-trip time of the laser cavity under injection (slave). The system consists of the carrier rate Eqs. (1)–(3) and the noise terms (5)–(7) and (10). In order to simulate a free-running laser, the injection terms in Eq. (9) should be neglected.

2.2. Time domain travelling-wave model

Although the RE model is a very efficient and accurate tool for investigating the majority of applications with semiconductor lasers, there are some cases that require even more sophisticated laser description. In particular, for the noise investigation of QCLs, a modified scheme of injection locking has been proposed and analysed by the authors; in this scheme, the injection of the master laser is carried out in a different than the dominant longitudinal mode of the slave laser. Such a configuration requires the description of the spectral characteristics of the laser, a property which can be treated easily by a travelling-wave (TW) model. The TW models can describe the multimode spectrum of a Fabry-Perot cavity and take into account the spectral profile of the material gain, both being necessary conditions in order to simulate the case of optical injection into secondary longitudinal modes. Furthermore, the TW models take into account the spatial distribution of the carriers and the field along the propagation direction, and thus they offer a more accurate description of the carrier dynamics in the gain medium than the RE models.

In the TW model, the carrier dynamics in the three-level QCL approximation shown in **Figure 1** is assumed to depend on the spatial coordinate z and is described by a set of two rate

equations [12, 13] for the carrier densities N_3 and N_2 [since no carrier loss between stages is assumed, the system is independent of N_1 and Eq. (3) may be neglected]:

$$\frac{dN_3}{dt} = \frac{\eta I}{q} - \frac{N_3}{\tau_{32}} - \frac{N_3}{\tau_{31}} - R_{st}(z,t) + F_3 \tag{11}$$

$$\frac{dN_2}{dt} = \frac{N_3}{\tau_{32}} - \frac{N_2}{\tau_{21}} + R_{st}(z,t) + F_2 \tag{12}$$

Here, the carrier numbers depend on the spatial coordinate z; thus, $N_3 = N_3(z,t)$ and $N_2 = N_2(z,t)$ are the local carrier numbers of the corresponding levels 3 and 2 between which the laser transition takes place; τ_{ij} is the characteristic transition time. The terms F_3 and F_2 represent the carrier noise, which follows the Langevin force formulation like in the RE model [Eqs. (5) and (6)], properly modified to account for the spatial dependence. The field propagation inside the active region is described by the travelling-wave equation for the forward and the backward slowly varying envelopes $E^{\pm}$ [11, 17]:

$$\frac{dE^{\pm}(z,t)}{dz} = \frac{1}{2}Zg(z,t)\left[\gamma e^{-\gamma t} \otimes E^{\pm}(z,t)\right] - i\frac{1}{2}Zg(z,t)\,\alpha_{LEF}\,E^{\pm}(z,t) - \frac{1}{2}a_l E^{\pm}(z,t) + \kappa_{DFB}\,E^{\mp}(z,t) + E_{sp}(z,t) \tag{13}$$

$E^{\pm}$ are the forward (+) and backward (−) propagating fields, g is the gain coefficient, Z is the number of cascaded gain stages, α_{LEF} is the linewidth enhancement factor and a_l is the total linear loss. g is the gain per unit length (m^{-1}) and depends on the carrier number of the levels 3 and 2:

$$g(z,t) = \frac{\Gamma g_0}{v_g}\left[N_3(z,t) - N_2(z,t)\right] \tag{14}$$

In Eq. (14), Γ is the confinement factor, v_g is the group velocity in the active region and g_0 is the differential gain constant in s^{-1}. The stimulated emission term in Eqs. (11) and (12) is given by

$$R_{st}(z,t) = \frac{g(z,t)V}{\hbar\omega \mathrm{wd}} \sum_{i=\pm} \Re\left\{E^{i*}(z,t)\left[\gamma e^{-\gamma t} \otimes E^{i}(z,t)\right]\right\} \tag{15}$$

The incorporation of a material gain profile with a finite spectral width in the travelling-wave equations is carried out by a filtering process in the time domain. Here, the gain profile is approximated with a Lorentzian function. As shown in Eqs. (13) and (15), the filtering process is described by the convolution product (symbol ⊗) of the field with the Lorentzian function of width γ. The operator $\Re()$ is the real part of a complex number. The simulation of multi-mode or single-mode operation is accomplished by adjusting the coefficient κ_{DFB} in Eq. (13), which represents the coupling between the forward and backward propagating waves due to the DFB grating in the waveguide. The term $E_{sp}(z,t)$ is the spontaneous emission noise per unit length; its expression is derived using the Langevin formulation of Ref. [10], and it is based on the spontaneous emission factor β (e.g. the coupling of the spontaneous emission to the lasing mode). Other parameters appear in **Table 1**.

The whole active region of length L is sliced into N sections of length dz each and Z stages with the same structure. The cavity effect and the optical injection of the master laser are modelled

Parameter	Symbol	Value
Active region length	L	2 mm
Active region width	w	8 μm
Active region depth	d	2 μm
Number of stages	Z	25
Facet power reflectivities	R_1, R_2	[0.27, 0.27]
Photon lifetime	τ_p	4.3 ps
Waveguide loss	a_l	1200 m^{-1}
Current injection efficiency	η	0.45
Gain coefficient	g	1.4×10^4 s^{-1}
Gain spectral width (FWHM)	γ	7 meV
Spontaneous emission factor	β	10^{-6}
Linewidth enhancement factor	α_{LEF}	0.5
Refractive index	n	3.2
Emission wavelength	λ	5 μm
Phonon scattering time $E_3 \rightarrow E_2$	τ_{32}	2.1 ps
Phonon scattering time $E_3 \rightarrow E_1$	τ_{31}	2.6 ps
Phonon scattering time $E_2 \rightarrow E_1$	τ_{21}	0.3 ps
DFB coupling coefficient	κ_{DFB}	10 m^{-1}
Injection coefficient (power)	κ_{inj}	Variable

Table 1. Physical and structural parameters used for the simulations of QCLs.

with boundary conditions. The solution of Eq. (13) is carried out in the time domain using an iterative algorithm to give the output field $E^+(L,t)$.

2.3. Noise calculations

The relative intensity noise (RIN) spectrum can be obtained from the output power fluctuations, and it is defined by

$$RIN(f) = \delta P(f)^2 / \langle P \rangle^2 \tag{16}$$

where P is the laser output power, f is the frequency, $\delta P(f)$ is the power fluctuations and the symbol $\langle \cdot \rangle$ represents the mean value. In the experiments, the RIN spectrum is calculated through Eq. (16) with the help of an electrical spectrum analyser (ESA). In the simulations, the instantaneous power fluctuations can be calculated from the output power of the laser in the time domain over a long time series with span T, as $\delta P(t) = P(t) - \langle P(t) \rangle$. The RIN spectrum then reads

$$RIN(\omega) = \frac{1}{\langle P(t)\rangle^2}\frac{1}{T}\left|\int_0^T \delta P(t)\, e^{-j\omega t}\, dt\right|^2 \tag{17}$$

Usually, the RIN value is calculated by averaging a narrow bandwidth at the low-frequency range where the spectrum is flat. Throughout this investigation, a single frequency window around 100 MHz has been used.

3. Intensity noise of free-running QCLs

The first step of the investigation regarding the intensity noise of injection-locked QCLs was to simulate the properties of a free-running QCL in order to confirm the validity of the RE model and the assumptions made for the contribution of the noise sources. Thus the RE model was used to simulate a single-mode QCL and compare the results with the corresponding results generated with the analytical theory of Gensty and Elsasser [12]. For this reason, all the parameters are taken from the work of Gensty and Elsasser [12] and shown in **Table 1**. **Figure 2** shows the RIN of the free-running QCL versus the output optical power (left) and the intensity noise spectrum in two cases (right). On the left side of **Figure 2**, the line corresponds to the analytical results generated with the theoretical model of Gensty and Elsasser [12], whereas the squares correspond to the numerical results generated by solving RE model under the same conditions. Both the analytical and numerical values of the RIN versus the optical power were obtained in the low-frequency range, and in the case of the RE model, a window of 150 MHz has been averaged. In order to reduce the statistical uncertainty due to the noise sources, the RIN value for each power level (current) is calculated by the average of 25 runs of the RE system with independent noise realizations.

As shown in **Figure 2**, the numerical results (squares) are in perfect agreement with the analytical ones (line), despite the simplifications made for the noise sources. This confirms the assumption that the dominant contributions to the total RIN come from the carriers in level 3 and the photons. The calculated intensity noise spectra for two different cases of output

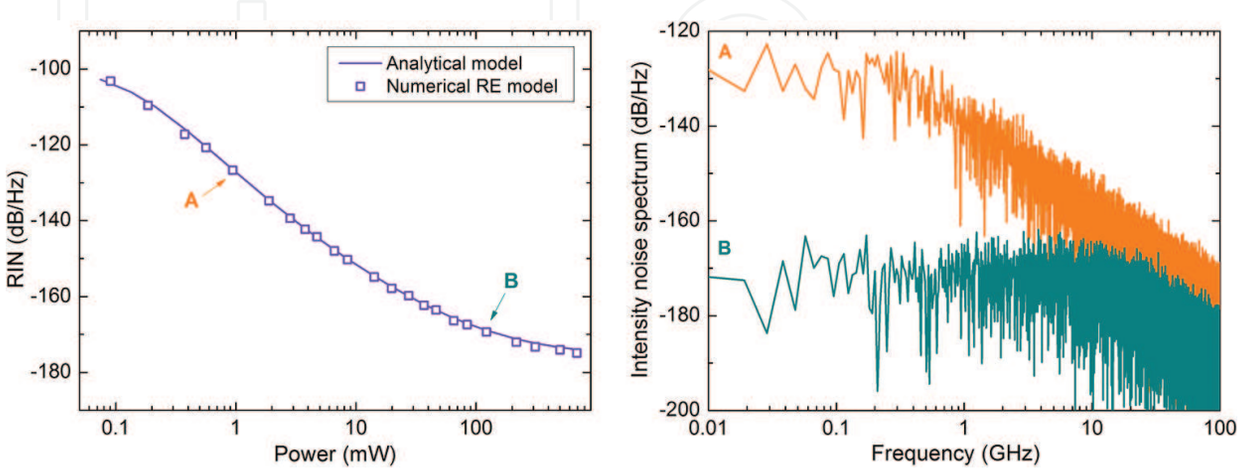

Figure 2. Left: The RIN of a free-running QCL versus the output optical power calculated with analytical (line) and numerical model (squares). Right: The intensity noise spectrum for two cases (points A and B of the RIN versus power curve).

optical power are also shown on the left of **Figure 2**. For low to moderate output power, the RIN spectrum is flat in the low-frequency regime (<1 GHz), and it fades out with frequency as shown by the spectrum of case A (top). In all cases, the spectrum in the low-frequency range and up to a few GHz is flat. Furthermore, the low-frequency plateau decreases with power, and the spectrum is flat up to a few tens of GHz as shown by the spectrum, which corresponds to case B (bottom). The flat low-frequency region and the disappearance of the resonance in the intensity noise spectrum are characteristics of damped carrier and thus photon relaxation oscillations. This behaviour is typical in QCLs in which the relaxation of the carriers is dominated by an ultrafast mechanism, the phonon scattering. This property is particular interesting for direct modulation and related applications which are modulation bandwidth demanding.

4. Intensity noise of injection-locked QCLs A: single-mode scheme

In this paragraph, the authors report the results of the investigation regarding the intensity noise properties in the most generic scheme of the injection locking method. In this scheme, the master and the slave QCLs are assumed to be ideal and emit in a single longitudinal mode; thus, the RE model was used for the simulations of the injection locking. The investigation is based on the effect of the two most important parameters of the injection locking process, the injection strength and the frequency detuning between the master and the slave laser.

4.1. Effect of the injection strength and the frequency detuning

By definition, the RIN properties of a laser are directly related to the emitted optical power, so it is reasonable to investigate first the injection process in terms of the output power. Furthermore, apart from the RIN, the role of the injected power from the master laser into the slave laser is significant on the locking process itself. **Figure 3a** illustrates the emitted optical power of the slave laser versus the current for different values of the injected optical power from the master laser (P_m), assuming the simplest case of zero master-slave frequency detuning (df = 0). A significant increase of the output power is observed below and right after the threshold current in all cases of injection compared to the free-running slave QCL case ($P_m = 0$). In the case of strong injection, the lasing threshold of the slave laser vanishes because of high injected power which turns on the lasing action in the slave laser, even if the current is very low. Essentially, the master laser acts as an optical pump for the slave laser, as it induces a huge increase of the photon number in the slave cavity. Above and close to the free-running threshold, the optical power of the slave laser gets even higher as the injected optical power increases. Furthermore, the power increase is practically minimized when moving away from the free-running threshold. Here, the emitted power is comparable with the power of the free-running slave laser.

Figure 3b illustrates the RIN levels of the slave laser over the entire range of the current corresponding to the conditions of **Figure 3a**. However, the RIN is plotted versus the emitted optical power of the slave laser instead of the current, in order to obtain a comparison of the RIN perfor-

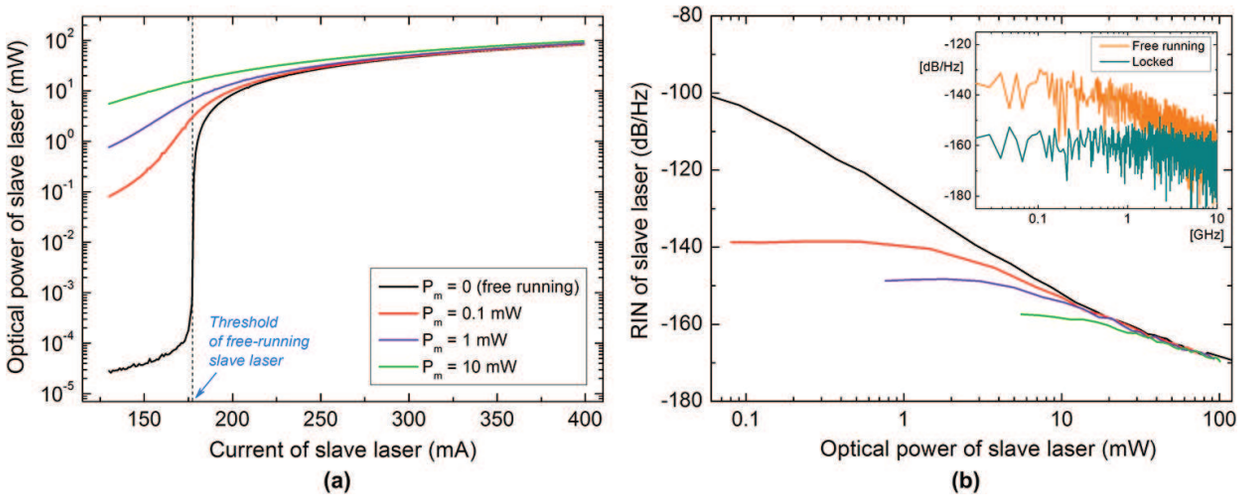

Figure 3. (a) The emitted optical power from the slave laser versus the injection current for different levels of the injected power from the master laser (P_m). (b) The RIN of the slave laser versus the emitted optical power. Insets show noise spectra of free-running and locked slave laser. In all cases, it is assumed zero frequency detuning between the master and slave lasers.

mance for different optical injections from the master laser but at the same output power levels. Additionally, a procedure for taking into account the right amounts of vacuum noise has been adopted for the calculations. The master QCL was driven at a high current to give the minimum possible RIN value of −175 dB/Hz, and its optical power was attenuated to the required values for injection to the slave laser. During every attenuation process, the degradation of the signal has been taken into account by introducing the vacuum noise properly. The resulting sets of (P_m, RIN) are (10 mW, −170 dB/Hz), (1 mW, −161 dB/Hz) and (0.1 mW, −151 dB/Hz).

As shown in **Figure 3b**, the RIN of the slave laser is reduced dramatically compared to the free-running values in all cases of injection. For low optical power of the slave laser (below and around the threshold current), the RIN is flat and is mainly determined by the injected power of the master laser and its intrinsic noise levels. The RIN gradually decreases with the output optical power, and up to a few mWs, it is still much lower than the corresponding free-running value. For current values far above threshold, the RIN reduction is saturated and similar to the free-running values are obtained. The inset of **Figure 3b** illustrates the intensity noise spectrum of the slave laser, in the case of free-running operation (orange line) and in the case of locked operation (cyan line), considering an injection power ratio (κ_{inj}) equal to 1 (1.7 mW). A suppression of ~20 dB on the low-frequency RIN of the locked slave laser is observed following the predictions of **Figure 3a**. However, as previously discussed, the actual RIN suppression is lower if compared to the same optical power, since the locking process results in a large power increase. Thus, in order to identify the actual noise performance, the RIN is always referenced/plotted at emitted power and not the current.

The RIN characteristics of the injection-locked QCLs can be explained with the help of the analytical calculations regarding the contribution of the different noise sources to the total RIN. As explained in Ref. [10], at the low output power regime (up to 5 mW in our case), the spontaneous emission of a free-running QCL (term R_{SS}) is unsaturated and dominant over the carrier noise (terms R_{33} and R_{22}). When photons are injected from the master laser, the spon-

http://dx.doi.org/10.5772/66941

taneous emission noise is suppressed significantly similar to what happens in bipolar semiconductor lasers; furthermore, since it is the dominant noise source, the total RIN is highly reduced compared to the free-running value. The situation is different in the high-power regime (far from the laser threshold) where the dominant contribution to the laser intensity noise comes from the carrier noise (R_{33}). Here, both the spontaneous emission noise and the carrier noise are already strongly saturated/suppressed. Therefore, in this case, the injection locking has very little or no effect on the RIN of the slave QCL. The domination of carrier noise in this regime imposes a fundamental limit on the potential RIN suppression achieved with injection locking directly on the oscillating mode of the QCL.

The frequency difference (detuning, df) between the master and the slave lasers is the other parameter that affects significantly the injection locking process. In detail, although the locking process can occur within a finite frequency detuning range between the two lasers, there is a dependence of the emitted power on the detuning which defines the so-called locking bandwidth of the process. Thus the locking bandwidth establishes the range of frequency difference between the two lasers in which the locking process is possible. In the case of QCLs, the locking bandwidth has been calculated analytically in previous works [7, 18] but with no correlation to noise properties. Here, the locking bandwidth is connected to the intensity noise of the emitted field from the slave QCL for various parameters. For this reason, in the calculations, an effective bandwidth was used, defined as the bandwidth of the noise reduction.

Figure 4a shows calculations of the optical power (red line) and the low-frequency RIN (violet circles) of the slave laser versus the frequency detuning between the master and slave lasers (df). The RIN distribution around the lasing mode is mapped with a large number of independent simulation runs in the investigated range (from −15 GHz to 15 GHz) with respect to the lasing frequency (0 GHz). For the calculations on the top of **Figure 4a**, the power of the free-running slave laser was P_{fr} = 10 mW (dashed black line) giving a RIN value of RIN_{fr} = −152 dB/Hz (the shadowed regions correspond to operation with RIN values below the free-running value). The injected power from the master laser was P_m = 1 mW (top left) and P_m = 10 mW (top

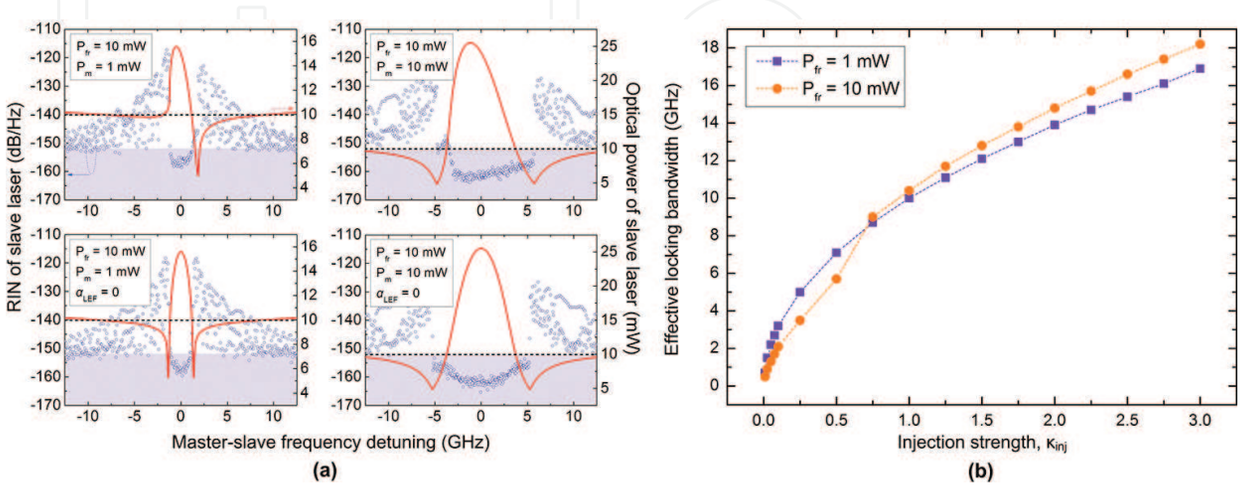

Figure 4. (a) The locking maps for two cases of injected power and (b) the effective locking bandwidth of the injection locking process.

right) having RIN values RIN_m = −161 dB/Hz and RIN_m = −170 dB/Hz, respectively. In both cases of injection, the bandwidth of the locking process can be extracted from the increased output power of the slave laser around the zero detuning. When low injection ratio is considered (κ_{inj} = 0.1, P_m = 1 mW), the locking occurs for ~2 GHz of frequency detuning and a reduction of the slave laser RIN in the order of 3–5 dB from the free-running value is observed. For frequencies outside the locking regime, the slave laser seems to operate in a "modulation" regime [19]. In this type of operation, the power is modulated as observed on the time traces and the corresponding RF spectra which exhibit peaks in the corresponding random frequencies. Such regimes most likely correspond to unstable locking, unlocked or chaotic oscillations, and they have been recently investigated in Ref. [20]. The asymmetry and the exact structure of the obtained locking map with respect to the difference in the negative and positive detuning are related to the non-zero linewidth enhancement factor [16]. Calculations under the same conditions but with a zero linewidth enhancement factor (α_{LEF} = 0) confirm this claim as the locking maps are perfectly symmetrical (bottom row of **Figure 4a**). When considering a higher injection ratio (κ_{inj} = 1, P_m = 10 mW), apparently the locking range is wider (~7 GHz) and the slave laser RIN is further reduced about ~10 dB with respect to the free-running case. Following the trend, the optical power of the slave laser is significantly increased compared to the case with κ_{inj} = 0.1.

Next, the effective locking bandwidth (defined as the bandwidth in which the slave QCL operates with lower noise than the free-running value) was calculated versus the injection strength, for different driving conditions of the slave QCL. Furthermore, in order to avoid the asymmetry of the locking region in the calculation of the effective bandwidth, the linewidth enhancement factor was set to zero (α_{LEF} = 0). The calculations have been carried out for P_{fr} = 1 mW and P_{fr} = 10 mW, and the results are plotted versus κ_{inj} in **Figure 4b**. In both cases, the effective locking bandwidth increases rapidly with the injections' strength. For low power of the slave QCL (P_{fr} = 1 mW), the injection locking gains more bandwidth in the low injection strength regime (κ_{inj} < 1) compared to the case of P_{fr} = 10 mW. In the high injection strength regime (κ_{inj} > 1), this behaviour is reversed since the locking process saturates earlier when the slave power is driven with low current.

4.2. Optimized noise operation in the single-mode injection locking scheme

With a second view to the locking maps of **Figure 4a**, a remarkable situation is revealed. The RIN of the slave laser within the locking range remains almost constant, whereas at the same time, the optical power is reduced significantly when moving towards the boundary regions. For example, in the case of P_{fr} = 10 mW (top right), close to the zero detuning (df = 0), the emitted power is 25 mW, and for detuning of 4 GHz, the emitted power is 8 mW. While the ratio in the optical power is 5 dB, the RIN changes only 2 dB, which indicates that there is operation with lower RIN under the same power levels. This observation leads to an important evidence: injection applied near the edges of the locking regime may drive the slave laser to operate under further reduced intensity noise due to the lower power. The actual RIN suppression which results from injection locking assuming the above conditions can be obtained with focusing on different locking regions with specific frequency detuning between the mas-

http://dx.doi.org/10.5772/66941

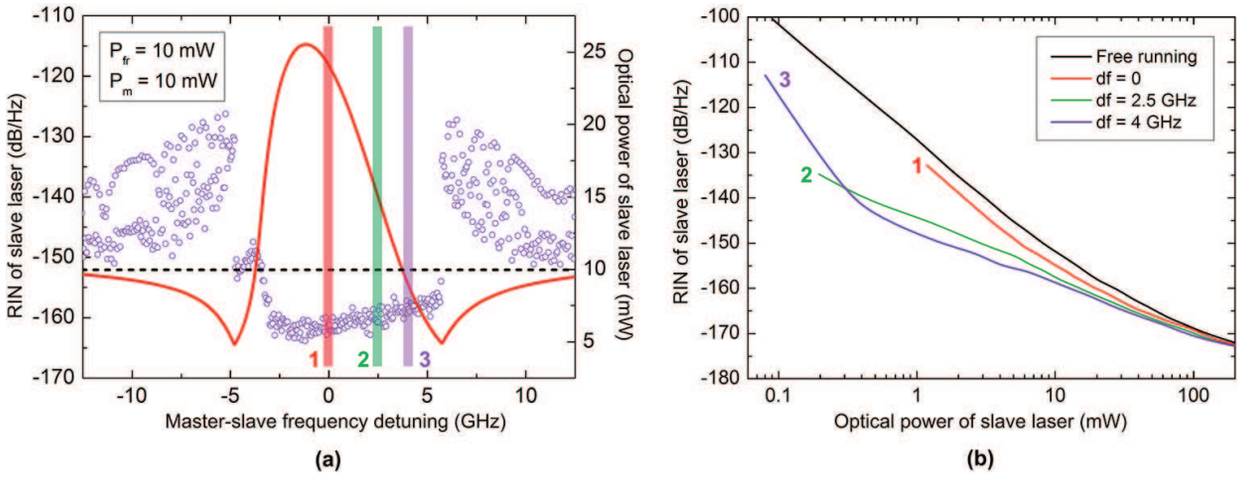

Figure 5. (a) The locking map indicating different regions with respect to the frequency difference between the master and the slave QCL and (b) the RIN of the slave laser under no injection and under injection locking at the frequency detuning values highlighted in (a).

ter and slave QCLs (df). To this end, the RIN of the slave laser was calculated versus the emitted optical power from the slave laser assuming a constant injection ratio instead of constant injected power in order to obtain RIN values of the slave laser in the low-power regime.

Figure 5 illustrates the results for $\kappa_{inj} = 1$ (the mean value of 25 independent runs). In the conventional case of injection locking directly on the lasing mode (df = 0), the RIN of the slave laser is constantly lower 4 dB than the free-running value up to 10 mW, however gradually approaching the free-running value, for even higher power (**Figure 5b**, red line). For injection in the second regime indicated in **Figure 5a** (df = 2.5 GHz), even lower RIN levels are observed before the saturation (**Figure 5b**, green line). In our analysis, the highest possible RIN suppression was found towards the positive edge of the locking regime (df = 4 GHz), where the RIN value was lower 21, 7 and 3 dB than the free-running value at 1, 10 and 50 mW of emitted power, respectively (**Figure 5b**, purple line).

5. Intensity noise of injection-locked QCLs B: multimode laser scheme

In the most common scheme of injection locking, the injection is realized in such a way that the wavelength of the master laser approximately matches the wavelength of the single-mode slave laser, e.g. injection into the lasing main longitudinal mode of a slave DFB laser. This technique has been adopted for the investigation of the previous paragraph. In addition to this scheme, several variations of the injection locking technique have revealed interesting characteristics in the case of interband diode lasers. For example, sub-shot noise performance (amplitude squeezing) has been achieved when optical injection is applied into a secondary longitudinal mode [21]. In order to optimize their properties, this method was applied to QCLs, and investigation of the noise properties and the locking potential has been carried out, as analysed in the next paragraphs.

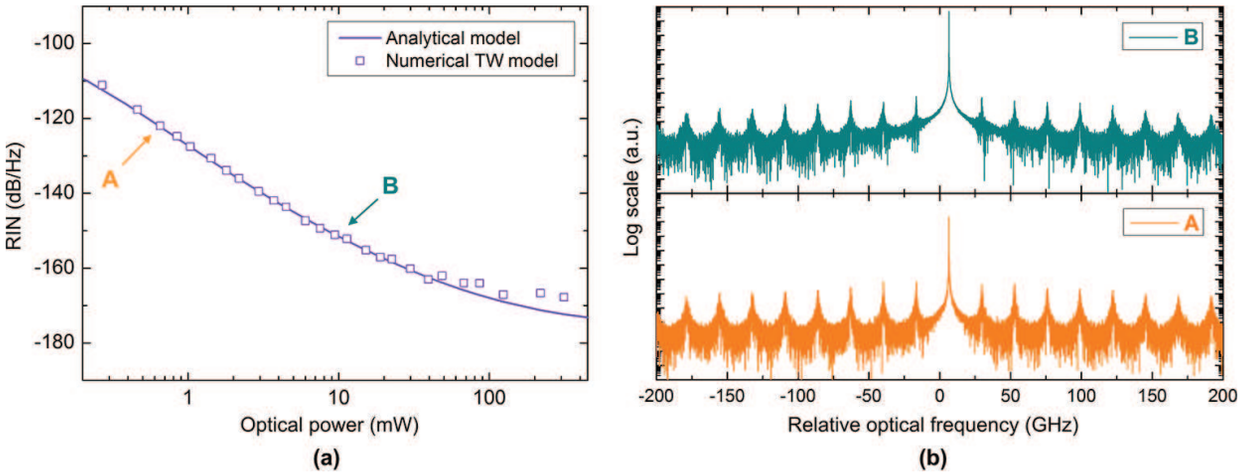

Figure 6. The RIN (a) and the optical spectrum (b) of the free-running QCL simulated with the TW model.

First, the TW model was used to reproduce the operation of a free-running QCL. **Figure 6a** illustrates the RIN of the free-running QCL simulated with both the TW and the analytical models with the parameters of the previous paragraph. The TW model is assumed to operate as a single-mode DFB laser, adjusting properly the grating coupling coefficient (κ_{DFB}). It is obvious that although the TW model is conceptually different from the RE model due to its inherent multi-longitudinal mode spectrum and the gain spectral profile, it reproduces fairly the noise characteristics of the single-mode QCL. As shown in **Figure 6b**, which illustrates the optical spectra in the two cases marked in **Figure 6a**, the side mode suppression ratio is very high even close to the threshold (spectrum on the bottom of **Figure 6b**).

Then, the TW model was used to investigate the noise properties of injection-locked QCLs with respect to the frequency detuning df. For this set of simulations, the power of the slave laser was set at 10 mW, and two cases of injection strength were considered: the master laser was driven at 1 and 10 mW (κ_{inj} = 0.1 and κ_{inj} = 1, respectively). In the case of injecting directly into the lasing mode (**Figure 7**, mode 0), the qualitative behaviour of the RIN with respect to the frequency detuning df is similar to the one generated with the RE model and analysed in the previous paragraphs. Here, the power and RIN profiles are asymmetrical with respect to the master-slave detuning, but also with respect to the zero frequency detuning due to the non-zero linewidth enhancement factor of the QCL. With higher injection the slave QCL exhibits higher locking bandwidth and optical power as well as lower noise in the locking range. Apart from this expected behaviour, the case of injection into a non-lasing secondary side mode was investigated. **Figure 7** demonstrates that the optical injection mechanism in a secondary mode (modes −1, +1) potentially leads to locking of the slave laser to the master wavelength and with similar characteristics (RIN, power), as in the case of injecting directly in the lasing mode. This is reasonable, since the adjacent to the lasing cavity modes is very close to the peak of the gain spectrum of the slave QCL, and the modes experience almost the same gain. The characteristics of injection on the main and the side modes have also been investigated experimentally and numerically by the authors in Ref. [11], and the results confirmed the

http://dx.doi.org/10.5772/66941

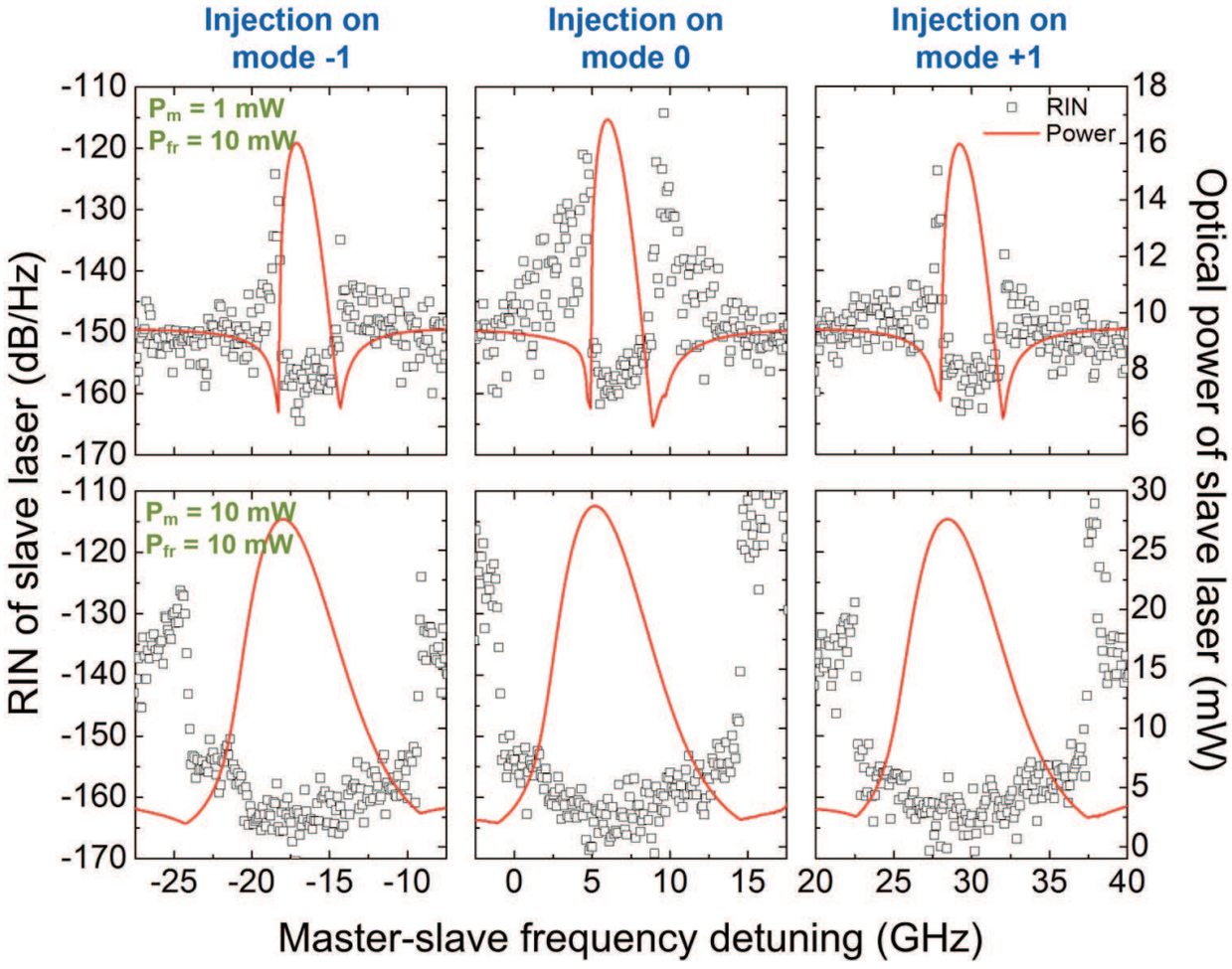

Figure 7. RIN and optical power of the slave QCL versus the frequency detuning for injection on the lasing (mode 0) and on the two adjacent longitudinal modes of the cavity (mode −1, +1).

results of this work. This is very important from the applications' point of view, since in practical conditions, it is not always easy to have QCLs (master-slave) emitting at the same wavelengths.

A more interesting and fundamentally different case occurs when the injection is realized into a resonant mode away from the gain peak of the slave QCL. This case has been simulated similarly to the previous cases but now for an extended master-slave frequency difference range of up to ±600 GHz in order to cover many of the modes within and outside the gain bandwidth. For this set of calculations, the power of the master and the same laser was the same, $P_{fr} = P_{ma} = 10$ mW. In order to give a better view, the RIN and the optical power of each of the simulated modes of the slave QCL have been plotted in **Figure 8** in a relative order showing their position within the optical spectrum and the gain profile of the laser. The red dashed line and the shadowed area denote the free-running value of the optical power (10 mW) and operation with lower RIN than the free running value (−152 dB/Hz), respectively.

The optical power of the slave QCL and the locking bandwidth fade slowly with the number of mode on which injection is carried out, due to the lower material gain available away

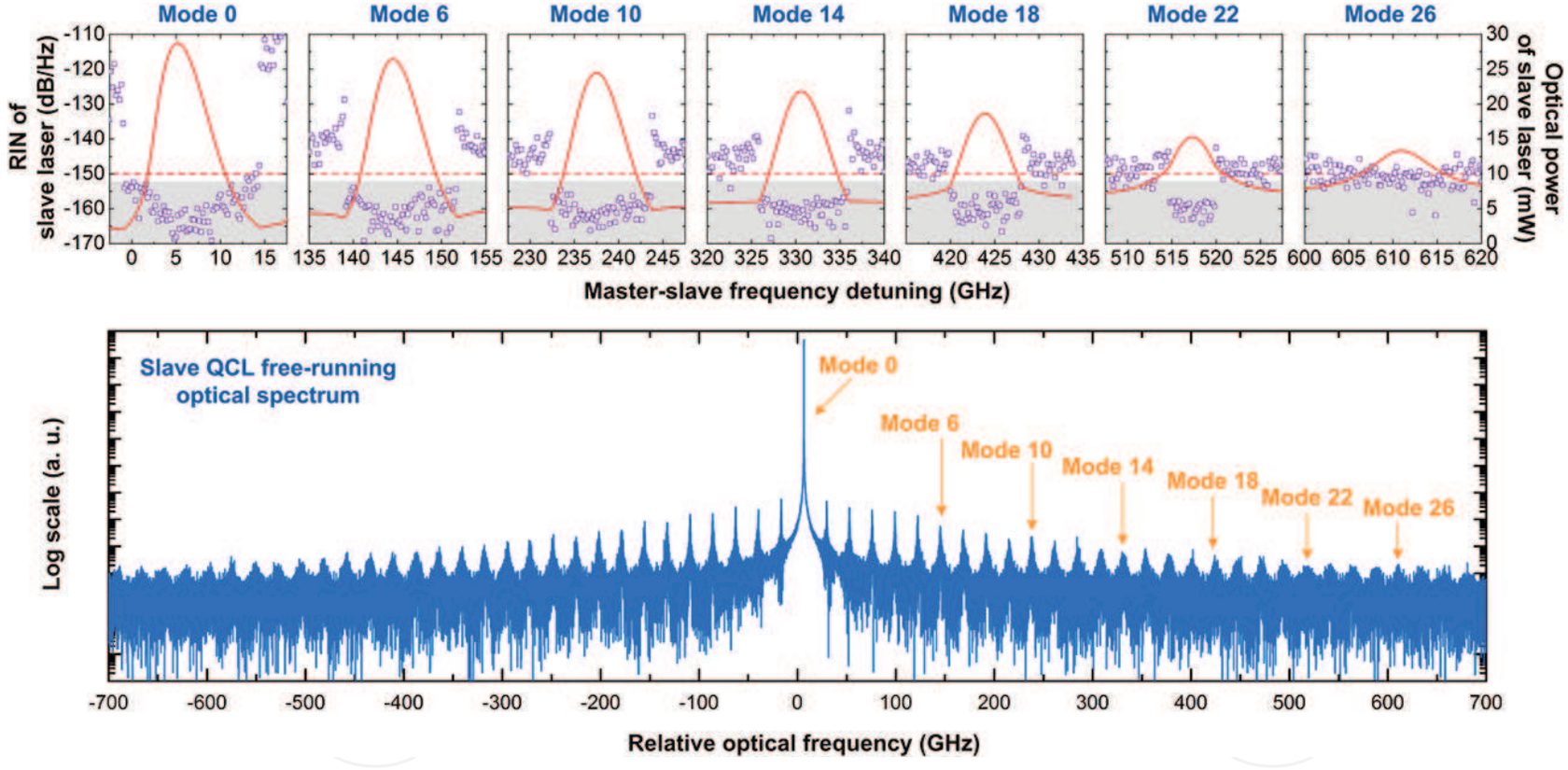

Figure 8. The RIN and the optical power versus the frequency detuning in the case of injection on different modes of the slave QCL.

http://dx.doi.org/10.5772/66941

of the gain peak. This characteristic is more intense after the 14th mode, as seen in **Figure 8**. Furthermore, for the same reason, the asymmetry of the locking characteristics with respect to the central frequency of each mode vanishes towards the edges of the spectrum. On the other hand, the RIN within the locking bandwidth is almost constant for many modes, as long as the injection locking takes place close to the peak of the gain spectrum of the slave laser. In detail, the lower average RIN within the locking bandwidth for all the modes up to the 10th is approximately −162 dB/Hz, whereas at the same time, the power decreases. Injection within the locking range of the above modes would result in a RIN suppression of ~10 dB compared to the free-running value. This finding provides us with a significant tool for optimization of the noise suppression, because similar RIN levels are achieved at lower optical power, which results in even higher actual RIN suppression (comparing RIN at the same optical power). This alternative type of injection locking provides stronger noise reduction as long as locking is applied on side modes which lie well within the gain bandwidth of the slave laser. This behaviour is similar to the one observed in the single-mode injection scheme (investigated with the RE model) where the RIN is much lower when the master laser is injected with a small detuning from the frequency of the slave laser (paragraph in Section 4.2). The same characteristics were observed for negative master-slave detuning.

In the case of injection outside of the gain bandwidth, although injection locking may fundamentally occur, the locking bandwidth is drastically reduced and the reduction potential of RIN is minimal. An indicative result is shown in **Figure 8** (mode +26).

6. Conclusions

According to the results reported in the previous paragraphs, for specific driving conditions, the injection locking has the ability to improve the RIN performance of a QCL laser. In summary, optical injection drives the slave laser to operate under simultaneous increased optical power and reduced RIN within the locking range, due to the suppression of the spontaneous emission noise and an increase of the photon number. This behaviour is dominant close to the threshold where spontaneous emission and phonon emission are the dominant noise factors. Far away from the threshold, the carrier noise from energy level 3 becomes stronger, and the total RIN suppression is lower, practically insignificant. Optimized low-noise operation was found with locking under frequency detuned injection between master and slave QCLs, resulting in significant actual RIN suppression (same RIN at lower emitted power) in the unsaturated regime (close to threshold). Furthermore, with an alternative scheme of injection locking on secondary modes of the slave QCL (not the free-running oscillation mode), it was observed that the RIN characteristics resemble the corresponding ones for injection on the main mode and may result in even further enhanced performance due to lower optical power. Based on the above investigation and the corresponding results, the injection locking process has been proven to be an efficient and practical technique to provide low-noise optical sources in the mid-IR region using quantum cascade lasers, which is critical for the majority of the sensing and spectroscopy applications.

Author details

Hercules Simos[1]*, Adonis Bogris[2] and Dimitris Syvridis[3]

*Address all correspondence to: simos@di.uoa.gr

1 Department of Electronics Engineering, Technological Educational Institute of Piraeus, Athens, Greece

2 Department of Informatics, Technological Educational Institute of Athens, Athens, Greece

3 Department of Informatics and Telecommunications, National and Kapodistrian University of Athens, Athens, Greece

References

[1] F. Capasso. High-performance midinfrared quantum cascade lasers. Optical Engineering. 2010;**49**(11):111102.

[2] J. Faist, F. Capasso, D. L. Sivco, C. Sirtori, A. L. Hutchinson, A. Y. Cho. Quantum cascade laser. Science. 1994;**264**(5158):553–556.

[3] S. Bartalini, S. Borri, P. Cancio, A. Castrillo, I. Galli, G. Giusfredi, D. Mazzotti, L. Gianfrani, P. De Natale. Observing the intrinsic linewidth of a quantum-cascade laser: beyond the Schawlow-Townes limit. Physical Review Letters. 2010;**104**(8):083904.

[4] F. P. Mezzapesa, L. L. Columbo, M. Brambilla, M. Dabbicco, S. Borri, M. S. Vitiello, H. E. Beere, D. A. Ritchie, G. Scamarcio. Intrinsic stability of quantum cascade lasers against optical feedback. Optics Express. 2013;**21**(11):13748–13757.

[5] T. Yang, G. Chen, C. Tian, R. Martini. Optical modulation of quantum cascade laser with optimized excitation wavelength. Optics Letters. 2013;**38**(8):1200–1202.

[6] A. Calvar, M. I. Amanti, M. Renaudat St-Jean, S. Barbieri, A. Bismuto, E. Gini, M. Beck, J. Faist, C. Sirtori. High frequency modulation of mid-infrared quantum cascade lasers embedded into microstrip line. Applied Physics Letters. 2013;**102**(18):181114.

[7] C. Wang, F. Grillot, V. Kovanis, J. Even. Nonlinear dynamics and modulation properties of optically injected quantum cascade lasers. In: CLEO/Europe - IQEC 2013; Munich, Germany. 2013.

[8] R. T. Ramos. Optical injection locking and phase-lock loop combined systems. Optics Letters. 1994;**19**(1):4–6.

[9] Y. Lai, H. A. Haus, Y. Yamamoto. Squeezed vacuum from amplitude squeezed states. Optics Letters. 1991;**16**(19):1517–1519.

[10] H. Simos, A. Bogris, D. Syvridis, W. Elsasser. Intensity noise properties of mid-infrared injection locked quantum cascade lasers: I. Modeling. IEEE Journal of Quantum Electronics. 2014;**50**(2):98–105.

[11] C. Juretzka, H. Simos, A. Bogris, D. Syvridis, W. Elsaber, M. Carras. Intensity noise properties of mid-infrared injection locked quantum cascade lasers: II. Experiments. IEEE Journal of Quantum Electronics. 2015;**51**(1):2300208.

[12] T. Gensty, W. Elsasser. Semiclassical model for the relative intensity noise of intersubband quantum cascade lasers. Optics Communications. 2005;**256**(1–3):171–183.

[13] F. Rana, R. J. Ram. Current noise and photon noise in quantum cascade lasers. Physical Review B. 2002;**65**(12):125313.

[14] T. Gensty, W. Elsasser, C. Mann. Intensity noise properties of quantum cascade lasers. Optics Express. 2005;**13**(6):2032–2039.

[15] N. Schunk, K. Petermann. Noise analysis of injection-locked semiconductor injection lasers. Noise analysis of injection-locked semiconductor injection lasers. IEEE Journal of Quantum Electronics. 1986;**22**(5):642–650.

[16] E. K. Lau, H.- K. Sung, M. C. Wu. Frequency response enhancement of optical injection-locked lasers. IEEE Journal of Quantum Electronics. 2008;**44**(1):90–99.

[17] M. Gioannini, M. Rossetti. Time-domain traveling wave model of quantum dot DFB lasers. IEEE Journal of Selected Topics in Quantum Electronics. 2011;**17**(5):1318–1326.

[18] B. Meng, Q. J. Wang. Theoretical investigation of injection-locked high modulation bandwidth quantum cascade lasers. Optics Express. 2012;**20**(2):1450–1464.

[19] I. Petitbon, P. Gallion, G. Debarge, C. Chabran. Locking bandwidth and relaxation oscillations of an injection-locked semiconductor laser. IEEE Journal of Quantum Electronics. 1988;**24**(2):148–154.

[20] T. Erneux, V. Kovanis, A. Gavrielides. Nonlinear dynamics of an injected quantum cascade laser. Physical Review E. 2013;**88**(3):032907.

[21] A. Furusawa. Amplitude squeezing of a semiconductor laser with light injection. Optics Letters. 1996;**21**(24):2014–2016.

IntechOpen